OPEN ACCESS

The 3rd World Sustainability Forum
1-30 November 2013

http://www.sciforum.net/conference/wsf3

Article, Review, Communication

Energy and Exergy Analyses of a New Combined Cycle for Producing Power and Pure Water Using Geothermal Energy

M. Akbari Kordlar [1], S.M.S. Mahmoudi [1] * and M.A. Rosen [2]

[1] Faculty of Mechanical Engineering, University of Tabriz, Daneshgah Street, Tabriz, Iran

[2] Faculty of Engineering and Applied Science, University of Ontario Institute of Technology, 2000 Simcoe Street North, Oshawa, Ontario L1H 7K4, Canada

mehri.akbari88@ms.tabrizu.ac.ir; s_mahmoudi@tabrizu.ac.ir; marc.rosen@uoit.ca

* Author to whom correspondence should be addressed; Tel.: 0098 411 3392487.

Received: 04 August 2013 / Accepted: 16 October 2013 / Published: 01 November 2013

Abstract: A new combined cogeneration system producing electrical power and pure water is proposed and analyzed thermodynamically. The system uses geothermal energy as a heat source and consists of a Kalina cycle, a LiBr/H_2O heat transformer and a water purification system. A parametric study is carried out in order to investigate the effects on system performance of the turbine inlet pressure and the evaporator exit temperature. For the proposed system, the first and second law efficiencies are found to be in the ranges of 16 - 18.2% and 61.9-69.1%, respectively. For a geothermal water stream with a mass flow rate of 89 kg/s and a temperature of 124^{o}C, the maximum production rate for pure water is found to be 0.367 kg/s.

Keywords: Geothermal energy, Kalina cycle, LiBr/H_2O heat transformer, Thermodynamic analysis, Thermoeconomic analysis

---

1. Introduction

The consumption of fossil fuels continues to increase to satisfy the increasing demand for energy and electricity in the world, leading to environment impacts and potential energy shortages. In order to

mitigate energy problems and protect the environment, increasing attention has been paid in recent years to the utilization of renewable energy and low-grade waste heat to generate power.

Amongst the renewable energies, geothermal sources have the highest availability since they are not dependent on weather conditions, and conversion technologies are available that allow electricity generation from geothermal fluids with low temperatures [1].

During the past 20 years various new thermodynamic cycles have been introduced and investigated. Some of these new cycles were designed to operate with medium or low temperature heat sources, and theoretical investigations have demonstrated the potential of these new cycles [2]. One of their characteristics is the use of a binary mixture as the working fluid, so as to increase thermal efficiency [3].

Binary component mixtures exhibit variable boiling temperatures during the boiling process. This allows for small temperature differences, and thus a good thermal match, between variable temperature heat sources and the working fluid, and consequently reduces irreversibility losses in the heat addition process [4]. The ammonia–water mixture is a typical binary mixture, which not only has excellent thermo-physical properties, but also is an environmentally-friendly material not causing ozone depletion. However, an ammonia–water mixture cannot be used in a power cycle directly, because the condensation process occurs at a variable temperature resulting in a higher turbine back pressure than that of the conventional steam Rankine cycle [5]. A higher turbine back pressure is of benefit for preventing air leakage into the system, but unfavorable in terms of power generation and cycle efficiency [6-7].

Maloney and Robertson [8] used an ammonia–water mixture as the working fluid in an absorption power cycle in the early 1950s. More recently, Kalina [9] proposed an absorption power cycle using ammonia-water. Maloney and Robertson concluded that the absorption power cycle has no thermodynamic advantage over the Rankine cycle, but Kalina[10] demonstrated that his cycle has a thermal efficiency which is 30-60% higher than comparable steam power cycles. By replacing the condensation process with an absorption process, Kalina [11] in 1984 solved the problem of higher turbine back pressure in combined cycles. Kalina and Leibowitz [12] explained the basic advantages of what has become known as the Kalina cycle technology. Also they presented a power cycle for geothermal applications. In that study, it was shown that the Kalina cycle has a higher power output for a specified geothermal heat source compared with organic Rankine cycles using iso-butane and steam flash cycles.

E1-Sayed and Tribus [13] compared the Rankine and Kalina cycles theoretically when both cycles are used as a bottoming cycle with the same thermal boundary conditions. They conducted first and second law thermodynamic analyses and concluded that the Kalina cycle can attain a 10-30% higher thermal efficiency than an equivalent Rankine cycle. Stecco and Desideri [14] analytically showed both thermodynamic and practical advantages for the Kalina cycle compared to a Rankine cycle using the exhaust of a gas turbine as an energy source. Marston [15] developed a computer model of the cycle analyzed by El-Sayed and Tribus. The results of this model show good agreement with published results of El-Sayed and Tribus.

The first prototype of the Kalina cycle was constructed in 1991. Nowadays, the Kalina cycle has been shown to achieve good performance results in diverse applications, e.g., in a geothermal plant built in Husavik, Iceland [16]. Currently, the Kalina cycle receives a great deal of attention for

numerous applications . Several Kalina cycle configurations exist, depending essentially on the heat source characteristics [17-18]:

- Kalina cycle system 5 (KSC5) is primarily focused on direct fired application,
- Kalina cycle system 6 (KCS6) is intended for use as the bottoming cycle in a combined cycle,
- Kalina cycle system 11 (KSC11) is particularly useful as a low temperature geothermal driven power cycle.
- Kalina cycle system 34 (KSC34) is used in low temperature geothermal power plants.

In 2007 Hettiarachchi [19] examined the performance of the Kalina cycle system 11 (KSC11) for low-temperature geothermal heat sources and compared it with an organic Rankine cycle. The results showed that, for a given turbine inlet pressure, an optimum ammonia fraction can be found that yields the maximum cycle efficiency. In general, KSC11 has better overall performance at moderate pressures than the organic Rankine cycle.

In 2009 LoLos [20] investigated a Kalina cycle using low-temperature heat sources to produce electricity. The main heat source of the cycle is flat solar collectors. In addition, an external heat source is connected to the cycle, which provides 5% to 10% of the total thermal energy supplied to the cycle.

Bombarda [21]compared the thermodynamic performances of a Kalina cycle and an organic Rankine cycle using hexamethyldisiloxane as the working fluid. This study was undertaken for the case of heat recovery from two Diesel engines, each producing an electrical power of 8900 kW. The maximum net electric power that can be produced using the heat source constituted by the exhaust gases mass flow rate (35 kg/s for both engines, at 346^{o}C) was calculated for the two thermodynamic cycles. Owing to the relatively low useful power, a relatively simple plant layout was assumed for the Kalina cycle.

Arslan [22] investigated electricity generation from the Simav geothermal field. The optimum operating conditions for the KCS-34 plant design were determined on the basis of exergetic and life-cycle-cost concepts. With the best design, a power generation of 41.2 MW and an electricity production of 346.1 GWh/a can be obtained with an energetic efficiency of 14.9% and exergetic efficiency of 36.2%. With current interest and inflation rates, the plant designs were shown to be economically feasible for values of the present worth factor (PWF) higher than six.

Ogresik [23] integrated the Kalina cycle in a combined heat and power plant to improve efficiency. In this analysis, the application of Kalina cycle system 34 was studied for low-temperature geothermal heat sources. This process raises the generated electricity with heat recovery and avoids the need for additional fuels, by integration in existing plants. The net efficiency of an integrated Kalina plant is shown to be between 12.3% and 17.1%, depending on the cooling water temperature and the ammonia content in the basic solution. The gross electrical power varies between 320 and 440 kW, for a 2.3 MW heat input rate to the process. The gross efficiency is between 13.5% and 18.8%. The study also showed that no more than half of the lost thermal energy in the bottoming cycle is recoverable. This thermal energy is rejected to the environment via an evaporator. The outlet temperature of the Kalina cycle in that evaporator, depending on the design and operating conditions, can vary between 75 and 80^{o}C. This temperature range could be a suitable for a LiBr/H_2O absorption heat transformer in seawater desalination applications (Sekar and Saravanan[24]; Rivera et al.[25]; Rivera et al.[26]; Gomri[27]; Gomri[28]; Rivera et al.[29]) but, according to our knowledge, this topic has not yet been investigated by researchers.

In this study, energy and exergy analyses and efficiency assessments are performed for the combined cycle. The exergy analysis is carried out to determine the irreversibility distribution within the plant and to determine the contribution of different components to the exergy destruction in the cycle. A parametric study is performed considering the effects of various design parameters on the cycle performance, with special attention paid to the effects of such parameters as turbine inlet pressure and evaporator exit temperature.

2. System description

The Kalina and LiBr/ H_2O cycles are described briefly before presenting proposed combined cycle.

2.1. Kalina cycle

Figure 1 shows a schematic diagram of the combined cycle. The working fluid is a mixture of ammonia and water. In the Kalina cycle, heat at a low temperature is transferred indirectly to a circulating fluid. The geothermal hot water (state point 13) enters the Kalina cycle evaporator (Evaporator 1) and causes the ammonia-water mixture to evaporate at state 5; the ammonia-water solution (with an ammonia mass fraction of 0.82) exits the evaporator and enters the separator, where the working fluid is separated into an ammonia-rich vapor and a weak solution. The ammonia-rich vapor, with an ammonia mass fraction of 0.96, passes through the turbine. The weak solution that did not vaporize in the evaporator leaves the separator as a saturated liquid at state 8 and passes to the high temperature (HT) recuperator. The ammonia-rich vapor after expansion through the turbine enters the mixing point, where it is mixed with the working fluid passing through the HT Recuperator. The mixed solution enters the low temperature (LT) Recuperator. In the LT Recuperator heat is exchanged with the cold stream coming from the pump. The hot stream leaving the LT Recuperator passes through the condenser where it is changed to a saturated liquid.

2.2. LiBr/H_2O absorption heat transformer cycle

The LiBr/H_2O absorption heat transformer processes are as follows: the saturated liquid at state 22 is subcooled in the heat exchanger, HEX, to state 23 and then is expanded to the low-side pressure, the generator. Heat is added in the generator from the geothermal stream, desorbing water vapor from the lithium bromide solution. The water leaves the generator as superheated vapor, the vapor is then condensed in the condenser before being pumped to the evaporator 2. The compressed liquid is heated in the evaporator 2 by the geothermal water and the obtained vapor passes to the absorber where it is absorbed by the solution coming from HEX. The heat of absorption is used to vaporize the sea water for purification purposes.

2.3. Combined cycle

The waste heat stream (states 13 to 17) is used to heat, evaporate and superheat the water (state 23). The superheated water at state 23 then combines with the concentrated lithium bromide-water solution at state 25, raising its temperature. As absorption of the vapor progresses to yield a dilute solution at

state 17, heat is rejected to the stream entering at state 28, heating it to state 30, and thereby providing the desired higher-grade heat output for seawater desalination. Note that in this configuration the waste heat stream is supplied in parallel rather than in series to the evaporator and generator.

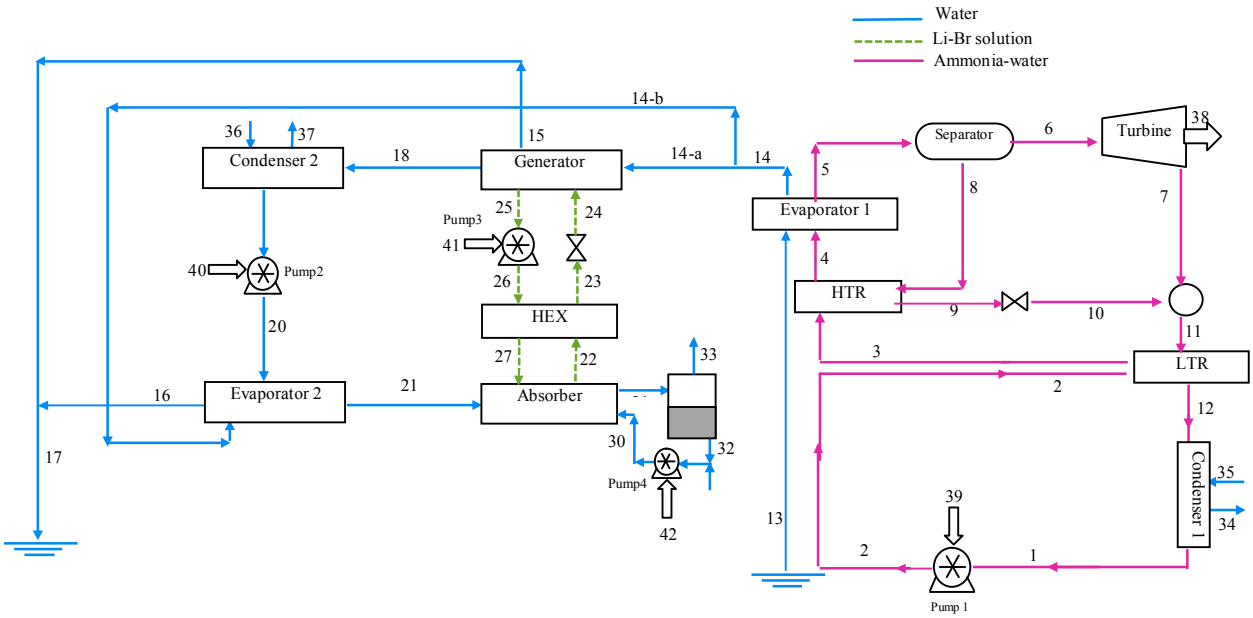

Figure 1: Schematic diagram of the combined cycle

3. Thermodynamic analysis

Thermodynamic models are developed for the Kalina and LiBr/H_2O cycles. In the models, each component of the system is treated as a control volume and the principle of mass conservation and the first and second laws of thermodynamics are applied to the component. Steady state operation is assumed throughout. Cycle performance is simulated by solving the corresponding equations together with the thermodynamic property relations in the EES software [30].

The mass rate balance for each component can be expressed as [31-33]:

$$\sum \dot{m}_{in} = \sum \dot{m}_{out} \tag{1}$$

Applying the first law of thermodynamics for each component yields the following energy rate balance:

$$\sum (\dot{m}h)_{in} - \sum (\dot{m}h)_{out} + \sum_j \dot{Q}_{cv} - \sum_k \dot{W}_{cv} = 0 \tag{2}$$

An exergy rate balance for each component of the system can be expressed as:

$$\sum \dot{E}_{in} - \sum \dot{E}_{out} + \dot{E}_{heat} + \sum_k \dot{W}_k = \dot{E}_{D,k} \tag{3}$$

In addition, the absorber and mixture is subject to an ammonia mass rate balance:

$$\sum (x\dot{m})_{in} = \sum (x\dot{m})_{out} \tag{4}$$

Here, the subscripts in and out denote inlet and exit states, $\dot{W}_{cv}$ is the electrical power output from the turbine reduced by the power input to the pump, $\dot{Q}_{cv}$ is the total heat rate addition to the cycle from the

heat source, $\dot{m}_i$ is the mass flow rate of the fluid, h is the specific enthalpy, $\dot{E}_D$ is the rate of exergy destruction, and $\dot{E}_{heat}$ is the net exergy transfer rate associated with heat transfer at temperature T, which is given by:

$$\dot{E}_{heat} = \sum_j \left(1 - \frac{T_0}{T_j}\right)\dot{Q}_j \tag{5}$$

In the absence of magnetic, electrical, nuclear and surface tension effects, and ignoring the kinetic and potential exergies, the total exergy rate of a stream becomes the sum of physical and chemical exergy rates [34]:

$$\dot{E} = \dot{E}_{ph} + \dot{E}_{ch} \tag{6}$$

The former can be obtained expressed as follows [34]:

$$\dot{E}_{ph} = \dot{m}\left[(h - h_0) - T_0(s - s_0)\right] \tag{7}$$

Here, the subscript 0 denotes the restricted dead state and T_0 the dead state temperature. The latter for the ammonia-water mixture and LiBr/H_2O can be evaluated as [35-36]:

$$\dot{E}_{ch(NH_3/H_2O)} = \dot{m}\left[\left(\frac{X}{M_{NH_3}}\right)e^0_{ch,NH_3} - T_0\left(\frac{1-X}{M_{H_2O}}\right)e^0_{ch,H_2O}\right] \tag{8}$$

$$\dot{E}_{ch(LiBr/H_2O)} = \dot{m}\left[\left(\frac{X}{M_{LiBr}}\right)e^0_{ch,LiBr} - T_0\left(\frac{1-X}{M_{H_2O}}\right)e^0_{ch,H_2O}\right] \tag{9}$$

In this analysis the change in chemical exergy of LiBr is not considered. This assumption, however, introduces a small error.

A detailed exergy analysis includes calculation of exergy destruction, exergy loss, exergetic efficiency, two exergy destruction ratios, and exergy loss ratio for each component of the system as well as the overall system. Mathematically, all these are expressed for the *k*th component as follows [34]:

$$\dot{E}_{D,k} = \dot{E}_{F,k} - \dot{E}_{P,k} - \dot{E}_{L,k} \tag{10}$$

$$\varepsilon_k = \frac{\dot{E}_{P,k}}{\dot{E}_{F,k}} = 1 - \left[\frac{(\dot{E}_{D,k} + \dot{E}_{F,k})}{\dot{E}_{F,k}}\right] \tag{11}$$

$$\dot{E}_{D,k} = \dot{E}_{F,k} - \dot{E}_{P,k} - \dot{E}_{L,k} \tag{12}$$

$$Y_{D,k} = \frac{\dot{E}_{D,k}}{\dot{E}_{F,total}} \tag{13}$$

$$Y^*_{D,k} = \frac{\dot{E}_{D,k}}{\sum_k \dot{E}_{D,total}} \tag{14}$$

$$Y_{L,k} = \frac{\dot{E}_{L,k}}{\dot{E}_{in,total}} \tag{15}$$

Mass, energy and exergy balances are provided in Table 1, along with the schematic of that particular component, where the flow streams are based on the states identified in Figure 1. The 'Fuel-Product-Loss' (F-P-L) definitions for the system are summarized in Table 2.

Table 1: Energy and exergy relations for the subsystems of the combined cycle

Subsystem	Exergy relation	Energy relation
Kalina cycle		
Evaporator 1	$E_{D,eva1} = T_0\left[m_4(s_5 - s_4) + m_{13}(s_{14} - s_{13})\right]$	$m_4(h_5 - h_4) = m_{13}(h_{14} - h_{13})$
Separator	$E_{D,\text{sep}} = T_0\left[m_6 s_6 + m_8 s_8 - m_5 s_5\right]$	$m_5 x_5 = m_6 x_6 + m_8 x_8$
Turbine	$E_{D,Tur} = T_0\left[m_6(s_6 - s_7)\right]$	$\eta_t = \frac{h_6 - h_7}{h_6 - h_{7s}}, w_t = m_6(h_6 - h_7)$
LTR	$E_{D,LTR} = T_0\left[m_{11}(s_{12} - s_{11}) + m_2(s_3 - s_2)\right]$	$m_2(h_3 - h_2) = m_{11}(h_{12} - h_{11})$
HTR	$E_{D,HTR} = T_0\left[m_3(s_4 - s_3) + m_8(s_9 - s_8)\right]$	$m_3(h_4 - h_3) = m_8(h_9 - h_8)$
Pump 1	$E_{D,P1} = T_0\left[m_1(s_2 - s_1)\right]$	$w_{p,1} = v_2(h_2 - h_1)$
Condenser 1	$E_{D,Con1} = T_0\left[m_1(s_1 - s_{12}) + m_{34}(s_{35} - s_{34})\right]$	$Q_{cond,1} = m_1(h_1 - h_{12})$
LiBr/H_2O cycle		
Evaporator 2	$E_{D,eva2} = T_0\left[m_{22}(s_{23} - s_{22}) + m_{15}(s_{15} - s_{13})\right]$	$m_{13}(h_{13} - h_{16}) = m_{22}(h_{22} - h_{23})$
Absorber	$E_{D,Abs} = T_0\left[(m_{17}s_{17} - m_{23}s_{23} - m_{26}s_{26}) + m_{29}(s_{30} - s_{29})\right]$	$m_{30}(h_{30} - h_{29}) = m_{17}h_{17} - m_{23}h_{23} - m_{26}h_{26}$
HEX	$E_{D,eva2} = T_0\left[m_{17}(s_{18} - s_{17}) + m_{25}(s_{26} - s_{25})\right]$	$m_{17}(h_{17} - h_{18}) = m_{25}(h_{25} - h_{26})$
Generator	$E_{D,Abs} = T_0\left[(m_{20}s_{20} - m_{24}s_{24} - m_{19}s_{19}) + m_{14}(s_{14} - s_{13})\right]$	$m_{13}(h_{13} - h_{16}) = m_{19}h_{19} - m_{20}h_{20} - m_{24}h_{24}$
Th. valve	$E_{D,\text{V}} = T_0\left[m_{24}(s_{25} - s_{24})\right]$	$m_{18}h_{18} = m_{19}h_{19}$
Pump 2	$E_{D,P2} = T_0\left[m_{21}(s_{22} - s_{21})\right]$	$w_{p,2} = v_{21}(h_{22} - h_{21})$
Pump 3	$E_{D,P3} = T_0\left[m_{24}(s_{25} - s_{24})\right]$	$w_{p,3} = v_{24}(h_{25} - h_{24})$
Pump 4	$E_{D,P4} = T_0\left[m_{28}(s_{29} - s_{28})\right]$	$w_{p,4} = v_{28}(h_{29} - h_{28})$
Condenser 2	$E_{D,Con2} = T_0\left[m_{20}(s_{21} - s_{20}) + m_{35}(s_{36} - s_{35})\right]$	$Q_{cond,2} = m_{20}(h_{20} - h_{21})$

Table 2: 'Fuel-Product-Loss' (F-P-L) definitions for the system

Subsystem	Fuel	Product
Kalina cycle		
Evaporator 1	$\dot{E}_{13} - \dot{E}_{14}$	$\dot{E}_5 - \dot{E}_4$
Turbine	$\dot{E}_6 - \dot{E}_7$	$\dot{W}_{Tur}$
LTR	$\dot{E}_{11} - \dot{E}_{12}$	$\dot{E}_3 - \dot{E}_2$
HTR	$\dot{E}_8 - \dot{E}_9$	$\dot{E}_4 - \dot{E}_3$
Pump 1	$\dot{W}_{P,1}$	$\dot{E}_2 - \dot{E}_1$
Condenser 1	$\dot{E}_{34} - \dot{E}_{35}$	$\dot{E}_{12} - \dot{E}_1$
LiBr/H_2O cycle		
Evaporator 2	$\dot{E}_{21} - \dot{E}_{20}$	$\dot{E}_{14-b} - \dot{E}_{16}$
Absorber	$\dot{E}_{31} - \dot{E}_{30}$	$(\dot{E}_{21} + \dot{E}_{27}) - \dot{E}_{22}$
HEX	$\dot{E}_{23} - \dot{E}_{22}$	$\dot{E}_{27} - \dot{E}_{26}$
Generator	$\dot{E}_{14} - \dot{E}_{15}$	$\dot{E}_{24} - (\dot{E}_{14} + \dot{E}_{18})$
Pump 2	$\dot{W}_{P,2}$	$\dot{E}_{20} - \dot{E}_{19}$
Pump 3	$\dot{W}_{P,3}$	$\dot{E}_{26} - \dot{E}_{25}$
Pump 4	$\dot{W}_{P,4}$	$\dot{E}_{30} - \dot{E}_{29}$
Condenser 2	$\dot{E}_{36} - \dot{E}_{37}$	$\dot{E}_{18} - \dot{E}_{19}$

3.1. Assumptions

The following assumptions are considered during this study [31]:

a) The geothermal power plants operate in a steady-state condition.

b) Pressure drops in heat exchangers and pipes are neglected.

c) The turbines and pumps have isentropic efficiencies.

d) Kinetic and potential energy changes are negligible.

e) The geofluid is in a saturated liquid condition in the reservoir ($x = 0$).

f) Thermodynamic properties of pure water have been used in the analysis for the geofluid.

g) Temperature and pressure losses of the geofluid are neglected in the separation and condensation processes.

3.2. Performance evaluation

For the combined cycle, the first law efficiency is referred to as the energy utilization efficiency, which is the ratio of useful energy output to the energy input. For the combined cycle in the present work, the energy utilization efficiency can be expressed as [31]:

$$\eta_{\mathrm{I}} = \frac{\dot{W}_{net} + \dot{Q}_{abs}}{\dot{Q}_{in}} \tag{16}$$

where

$$\dot{W}_{net} = \dot{W}_{Tur} - (\dot{W}_{P,1} + \dot{W}_{P,2} + \dot{W}_{P,3} + \dot{W}_{P,4}) \tag{17}$$

$$\dot{Q}_{abs} = m_{30}(h_{31} - h_{30}) \tag{18}$$

$$\dot{Q}_{in} = m_{1}(h_{1} - h_{17}) \tag{19}$$

Similarly, the second law efficiency of the combined cycle can be defined as:

$$\eta_{\mathrm{II}} = \frac{\dot{W}_{net} + \dot{E}_{abs}}{\dot{E}_{in}} \tag{20}$$

where

$$\dot{E}_{abs} = \dot{E}_{31} - \dot{E}_{30} \tag{21}$$

$$\dot{E}_{in} = m_{1}\left[(h_{1} - h_{17}) - T_{0}(s_{1} - s_{17})\right] \tag{22}$$

3.3. Model validation

Data available in the literature are used to validate the simulation. For the case of the Kalina cycle, the numerical model was validated by using previously published data [23]. Figure 2 shows the result of the validation. Similarly, Figure 3 shows the results of the validation of absorption heat transformer cycle using data from Rivera et al [29].

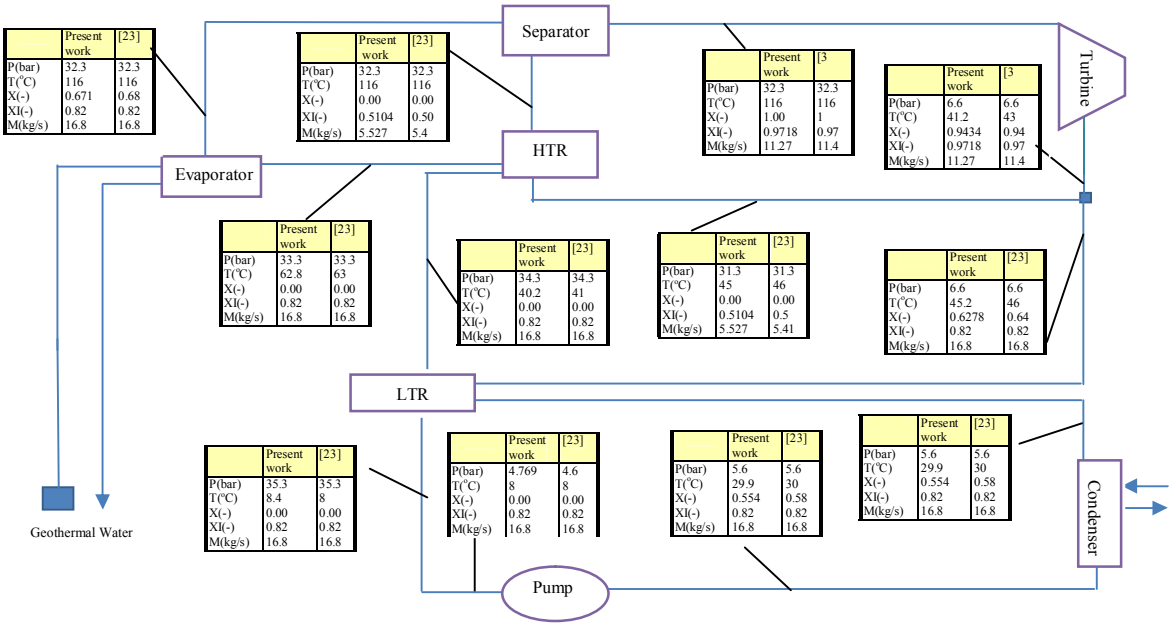

Figure 2: Comparison of present simulation results and those from previously published work, for the thermodynamic state of the Kalina cycle

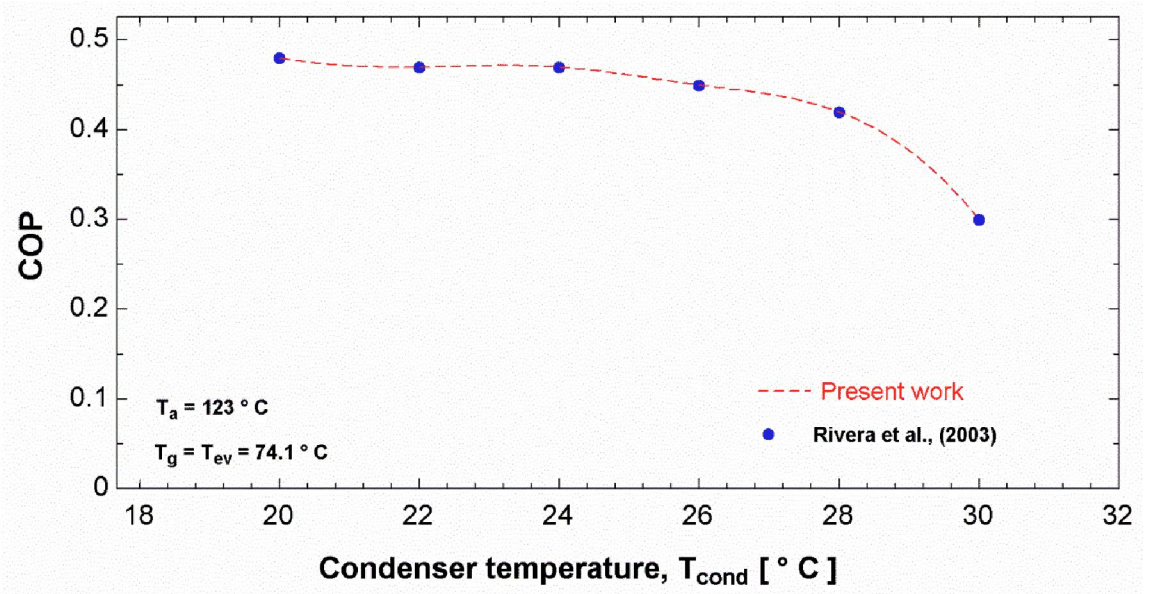

Figure 3: Comparison between the present simulation results and those of Rivera et al. [29] for the coefficient of performance (COP) of the absorption heat transformer system

4. Thermoeconomic analysis

The aim of thermoeconomic analysis is to reveal the cost formation processes and calculate the cost per exergy unit of the product streams of the system. The unit exergetic cost of the products obtained from this procedure is used for economic optimization of the cycle. In order to calculate the unit cost of each exergy stream, a cost balance along with the required auxiliary equations are applied to each

component of the cycle. For a system component receiving thermal energy and generating power, the cost rate balance may be written as [34]:

$$\sum \dot{C}_{out,k} + \dot{C}_{w,k} = \sum \dot{C}_{in,k} + \dot{C}_{q,k} + \dot{Z}_k \tag{23}$$

where

$$\dot{C} = c\dot{E} \tag{24}$$

snd c is the cost per unit of each exergy stream. The terms $\dot{C}_{w,k}$ and $\dot{C}_{q,k}$ are the cost rates associated with the output power from the component and input thermal energy to the component, respectively. Eq. (24) states that the total cost rate of exiting exergy streams equals the total cost rate of entering exergy streams plus the total expenditure rate to accomplish the process.

The term $\dot{Z}_k$ in Eq. (25) is the total cost rate associated with capital investment and operation and maintenance for the kth component:

$$\dot{Z}_k = \dot{Z}_k^{CI} + \dot{Z}_k^{OM} \tag{25}$$

The annual levelized capital investment for the kth component can be calculated as [34]:

$$\dot{Z}_k^{CI} = (\frac{CRF}{\tau}) Z_k \tag{26}$$

where CRF and τ are the capital recovery factor and the annual plant operation hours, respectively. The capital recovery factor is a function of the interest rate i_r and the number of useful years of plant operation n [28]:

$$CRF = \frac{i_r (1+i_r)^n}{(1+i_r)^n - 1} \tag{27}$$

The calculation of Z_k for each component of the system is given in Appendix A. The annual levelized operation and maintenance cost for the kth component are calculated as:

$$\dot{Z}_k^{OM} = \gamma_k Z_k + \omega_k \dot{E}_{P,k} + \dot{R}_k \tag{28}$$

where γ_k and ω_k account for the fixed and variable operation and maintenance costs, respectively, associated with the kth component and $\dot{R}_k$ includes all the other operation and maintenance costs which are independent of investment cost and product exergy. Since the last two terms on the right side of the equation are small compared to the first one, these terms may be neglected as is done by some other researchers [34-36].

The formulation of cost rate balance and required auxiliary equations for each component of the cycle leads to the following system of equations:

Evaporator 1:

$$\dot{C}_5 + \dot{C}_{14} = \dot{Z}_{eva,1} + \dot{C}_4 + \dot{C}_{13} \tag{29}$$

$$\frac{\dot{C}_{13}}{\dot{E}_{13}} = \frac{\dot{C}_{14}}{\dot{E}_{14}} \quad \text{or} \quad c_{13} = c_{14} \tag{30}$$

Separator and valve:

$$\dot{C}_6 + \dot{C}_8 + \dot{C}_{10} = \dot{Z}_{sep\&vale,1} + \dot{C}_5 + \dot{C}_9 \tag{31}$$

$$\frac{\dot{C}_6 - \dot{C}_5}{\dot{E}_6 - \dot{E}_5} = \frac{\dot{C}_8 - \dot{C}_5}{\dot{E}_8 - \dot{E}_5} \tag{32}$$

$$\frac{\dot{C}_9}{\dot{E}_9} = \frac{\dot{C}_{10}}{\dot{E}_{10}} \quad \text{or} \quad c_9 = c_{10} \tag{33}$$

Turbine:

$$\dot{C}_7 + \dot{C}_{38} = \dot{Z}_{Tur} + \dot{C}_6 \tag{34}$$

$$\frac{\dot{C}_6}{\dot{E}_6} = \frac{\dot{C}_7}{\dot{E}_7} \quad \text{or} \quad c_6 = c_7 \tag{35}$$

LTR:

$$\dot{C}_3 + \dot{C}_{12} = \dot{Z}_{LTR} + \dot{C}_2 + \dot{C}_{11} \tag{36}$$

$$\frac{\dot{C}_{11}}{\dot{E}_{11}} = \frac{\dot{C}_{12}}{\dot{E}_{12}} \quad \text{or} \quad c_{11} = c_{12} \tag{37}$$

HTR:

$$\dot{C}_4 + \dot{C}_9 = \dot{Z}_{HTR} + \dot{C}_3 + \dot{C}_8 \tag{38}$$

$$\frac{\dot{C}_8}{\dot{E}_8} = \frac{\dot{C}_9}{\dot{E}_9} \quad \text{or} \quad c_8 = c_9 \tag{39}$$

Pump 1:

$$\dot{C}_2 = \dot{Z}_{P,1} + \dot{C}_1 + \dot{C}_{39} \tag{40}$$

Condenser 1:

$$\dot{C}_1 + \dot{C}_{35} = \dot{Z}_{cond,1} + \dot{C}_{12} + \dot{C}_{34} \tag{41}$$

$$\frac{\dot{C}_1}{\dot{E}_1} = \frac{\dot{C}_{12}}{\dot{E}_{12}} \quad \text{or} \quad c_1 = c_{12} \tag{42}$$

Evaporator 2:

$$\dot{C}_{16} + \dot{C}_{21} = \dot{Z}_{eva,2} + \dot{C}_{14-b} + \dot{C}_{20} \tag{43}$$

$$\frac{\dot{C}_{14-b}}{\dot{E}_{14-b}} = \frac{\dot{C}_{16}}{\dot{E}_{16}} \quad \text{or} \quad c_{14} = c_{16} \tag{44}$$

Absorber:

$$\dot{C}_{22} + \dot{C}_{31} = \dot{Z}_{Abs} + \dot{C}_{21} + \dot{C}_{27} + \dot{C}_{30} \tag{45}$$

$$\frac{\dot{C}_{21} + \dot{C}_{27}}{\dot{E}_{21} + \dot{E}_{27}} = \frac{\dot{C}_{22}}{\dot{E}_{22}} \tag{46}$$

HEX:

$$\dot{C}_{23} + \dot{C}_{27} = \dot{Z}_{HEX} + \dot{C}_{22} + \dot{C}_{26} \tag{47}$$

$$\frac{\dot{C}_{22}}{\dot{E}_{22}} = \frac{\dot{C}_{23}}{\dot{E}_{23}} \quad \text{or} \quad c_{22} = c_{23} \tag{48}$$

Generator:

$$\dot{C}_{15} + \dot{C}_{18} + \dot{C}_{25} = \dot{Z}_{Gen} + \dot{C}_{14-a} + \dot{C}_{24} \tag{49}$$

$$\frac{\dot{C}_{18}-\dot{C}_{24}}{\dot{E}_{18}-\dot{E}_{24}}=\frac{\dot{C}_{25}-\dot{C}_{24}}{\dot{E}_{25}-\dot{E}_{24}} \quad (50)$$

$$\frac{\dot{C}_{14-a}}{\dot{E}_{14-a}}=\frac{\dot{C}_{15}}{\dot{E}_{15}} \quad \text{or} \quad c_{14-a}=c_{15} \quad (51)$$

Condenser 2:

$$\dot{C}_{19}+\dot{C}_{37}=\dot{Z}_{cond,2}+\dot{C}_{18}+\dot{C}_{36} \quad (52)$$

$$\frac{\dot{C}_{18}}{\dot{E}_1 8}=\frac{\dot{C}_{19}}{\dot{E}_{19}} \quad \text{or} \quad c_{18}=c_{19} \quad (53)$$

Pump 2:

$$\dot{C}_{20}=\dot{Z}_{P,2}+\dot{C}_{19}+\dot{C}_{40} \quad (54)$$

Pump 3:

$$\dot{C}_{26}=\dot{Z}_{P,3}+\dot{C}_{25}+\dot{C}_{41} \quad (55)$$

Pump 4:

$$\dot{C}_{30}=\dot{Z}_{P,4}+\dot{C}_{29}+\dot{C}_{42} \quad (56)$$

The linear system of equations in Eqs. (29)-(56) include 42 unknown variables: $[\mathrm{X}]=\{\dot{\mathrm{C}}_1,\dot{\mathrm{C}}_2,...\}$. Assuming a known value for the unit exergetic cost of the geothermal source ($c_{13}=1.3$) and considering the fact that the unit exergetic cost of the cooling water can be neglected [29], i.e., $c_{33}=0$, $c_{35}=0$ and $c_{27}=0$. Also we have $c_{14-a}=c_{14-b}=c_{14}$ and $\dot{C}_{14}=\dot{C}_{14-a}+\dot{C}_{14-b}$, making it possible to obtain the unit exergetic cost of all exergy streams of the system by solving the system of 42 equations and 42 unknowns.

5. Results and discussions

The parametric analysis is performed to evaluate the effects of each major parameter, namely, turbine inlet pressure (P_6), evaporator exit ammonia concentration (X_5) and evaporator exit water temperature (T_{14}) on parameters related to the combined cycle performance, such as thermal and exergy efficiencies and the sum of the unit cost of the products. When one specific parameter is examined, the other parameters are kept constant, as shown in Table 1.

The basic assumption and input parameters used in the study are given in Table 3. As mentioned in Section, the input energy to the system is provided by means of saturated steam. Table 4 shows the results of thermodynamic simulation. Table 5 summarizes the calculated thermodynamic properties along with the cost flow rates and unit costs at various state points of the system for the base case operating conditions and Table 6 summarizes the exergy analysis of the system, which is carried out using F-P-L relationships and Eqs. (27)-(28)

Table 3: Input data assumed in the simulation

Temperature of the reference environment	25°C
Pressure of the reference environment	1 bar
Temperature of water from the well	124°C
Temperature of exit water of Evaporator 1	80°C
Turbine inlet pressure	32.3bar
Temperature of water to the well	T_{14}-5
Temperature of solution exiting condenser	T_0+5
Temperature of Generator and Evaporator 2	T_{16}-3
Mass flow rate of geothermal water	89 kg/s
Temperature of LiBr/H_2O solution	110°C
Mass flow rate of seawater	12 kg/s
Ammonia mass fraction	82%
Turbine isentropic efficiency	90%
Pump isentropic efficiency	80%

Table 4: Performance of the combined cycle

Turbine work rate (kW)	2452
Condenser 1 heat rejection rate (kW)	14172
Pump 1 work rate (kW)	80.59
Pump 2 work rate (kW)	0.01203
Pump 3 work rate (kW)	83.04
Pump 4 work rate (kW)	0.1108
Evaporator 1 heat input rate (kW)	16543
Evaporator 2 heat input rate (kW)	1009
Absorber heat transfer rate (kW)	938.3
Generator heat transfer rate (kW)	857.3
Condenser 2 heat rejection rate (kW)	1011
Net power output of Kalina cycle (kW)	2371
Net power output and absorber heat rate (kW)	3226
Heat input rate (kW)	18409
Exergy input rate (kW)	3676
Thermal efficiency (%)	17.52
Exergy efficiency (%)	67.38

Table 5: Thermodynamic properties and cost of streams for the combined cycle

State	T ($^{\circ}C$)	P (bar)	X	(kg/s)	$\dot{E}_{ph}$ (kJ/kg)	$\dot{E}_{ch}$ (kJ/kg K)	$\dot{E}$ (kW)	$\dot{C}$ ($/h)	C ($/GJ)
1	20	7.124	0	17.82	3,100	289,132	292,231	2455	2.333
2	20.6	32.3	-	17.82	3,164	289,132	292,295	2455	2.333
3	44.6	32.3	-	17.82	3,214	289,132	292,345	2457	2.335
4	65.6	32.3	-	17.82	3,382	289,132	292,513	2460	2.337
5	118	32.3	0.6824	17.82	6,388	289,132	295,520	2480	2.331
6	118	32.3	1	12.16	5,915	233,147	239,065	2007	2.332
7	46.4	7.124	0.9417	12.16	3,212	233,147	236,359	1984	2.332
8	118	32.3	0	5.658	470.4	55,984	56,455	475.4	2.339
9	49.6	32.3	-	5.658	170.8	55,984	56,155	472.9	2.339
10	50	7.124	-	5.658	154.5	55,984	56,139	472.7	2.339
11	49.6	7.124	0.6382	17.82	3,364	289,132	292,496	2457	2.333
12	40.4	7.124	0.5778	17.82	3,228	289,132	292,359	2456	2.333
13	124	2.25	-	89	5,085	0	5,085	23.8	1.3
14	80	2.25	-	89	1,689	0	1,689	7.906	1.3
14-a	80	2.25	-	40.89	913.2	0	913.2	4.274	1.3
14-b	80	2.25	-	48.11	776	0	776	3.632	1.3
15	75	2.25	-	40.89	647.4	0	647.4	3.03	1.3
16	75	2.25	-	48.11	761.8	0	761.8	3.565	
17	75	2.25	-	89	1,409	0	1,409	6.595	1.3
18	72	0.04246	-	0.4029	18.74	0	18.74	4.012	59.48
19	30	0.04246	-	0.4029	0.07032		0.07032	0.01506	59.48
20	30	0.3397	-	0.4029	0.08235	0	0.08235	0.02232	75.29
21	72	0.3397	-	0.4029	134.4	0	134.4	1.224	2.529
22	110	0.3397	0.5511	5.034	229.5	5.643	235.2	5.979	7.063
23	92.73	0.3397	0.5511	5.034	193.1	5.643	198.8	5.055	7.063
24	64.72	0.04246	0.5511	5.034	439.2	5.643	439.2	11.31	7.063
25	72	0.04246	0.5982	4.631	274.1	4.647	278.8	8.466	8.437
26	81.27	0.3397	0.5982	4.631	286.8	4.647	291.5	9.307	8.87
27	101.4	0.3397	0.5982	4.631	319.7	4.647	324.3	10.44	8.942
28	25	1	-	0.365	0.03545	0	0.03545	0	0
29	98.19	0.9494	-	15	488.1	0	488.1	20.4	11.61
30	98.19	1.013	-	15	488.3	0	488.3	20.41	11.61
31	100	1.013	-	15	676.6	0	676.6	27.19	11.15
32	100	1.013	-	14.67	498.6	0	498.6	20.4	11.36
33	100	1.013	-	0.365	178	0	178	8.255	12.82
34	15	1	0	677.5	485.2	0	485.2	0	0
35	20	1	-	677.5	119.6	0	119.6	3.28	7.617
36	15	1	-	48.33	34.61	0	34.61	0	0
37	20	1	-	48.33	8.532	0	8.532	4.246	138.2
38	-	-	-	-	-	-	2452	22.74	2.257
39	-	-	-	-	-	-	80.59	0.7473	2.256
40	-	-	-	-	-	-	0.01203	0.00011	2.576
41	-	-	-	-	-	-	83.04	0.7701	2.576
42	-	-	-	-	-	-	0.1108	0.00102	2.576

Table 6: Cost analysis results for combined cycle

Subsystem	$\dot{E}_{F,k}$ (kW)	$\dot{E}_{P,k}$ (kW)	$\dot{E}_{D,k}$ (kW)	$Y_{D,k}$ (%)	$Y^{*}_{D,k}$ (%)	ε_k (%)
Kalina cycle						
Evaporator 1	3396	3007	389	4.71	24.46	88.54
Turbine	2706	2452	254	3.06	15.97	90.61
LTR	137	50	87	1.04	5.47	36.49
HTR	300	168	132	1.59	0.1	56
Separator and valve	316	300	16	0.19	1.006	94.93
Pump 1	80.59	64	16.59	0.19	1.04	79.41
Condenser 1	364.6	128	236.6	2.85	14.88	35.1
$LiBr/H_2O$ cycle						
Evaporator 2	134.31	14.2	118.31	1.42	7.44	10.57
Absorber	223.5	188.5	35	0.42	2.20	84.34
HEX	36.4	32.8	3.6	0.04	0.22	90.1
Generator	492.74	265.8	226.94	2.73	14.27	53.94
Pump 2	0.01204	0.01203	0.0001			
Pump 3	83.04	12.7	70.34	0.84	4.42	15.3
Pump 4	0.1108	0.11	0.0008			
Condenser 2	26.078	18.66	4.418	0.05	0.27	71.55
Overall system	8296.4	6701.8	1589.8	19.16	100	80.77

Figure 4 shows the effect of turbine inlet pressure on the first law efficiencies of the Kalina and combined cycles for various hot water temperatures exiting Evaporator 1. For each temperature, an optimum pressure is observed to exist at which the first law efficiency is maximized.

The trend of first law efficiency in Figure 4 can be justified considering the results in Figs. 5, 6 and 7. As Figure 5 indicates, the specific enthalpy values at the turbine inlet and exit decrease with temperature. The amounts of reductions, however, are such that the difference between the two specific enthalpy values is maximized at a pressure of around 52 bar. The results also indicate that for a known value of the Evaporator 1 temperature, an increase in turbine inlet pressure causes a reduction in the turbine mass flow rate (Figure 8). Figure 6 also shows that, considering the change in pump power, the cycle net output power decreases as the turbine inlet pressure increases.

It is observed in Figure 7 that as the turbine inlet pressure increases, the cycle input heat rate decreases. The rate of decrease in net output power, however, is such that the first law efficiency is maximized at a particular value of turbine inlet pressure.

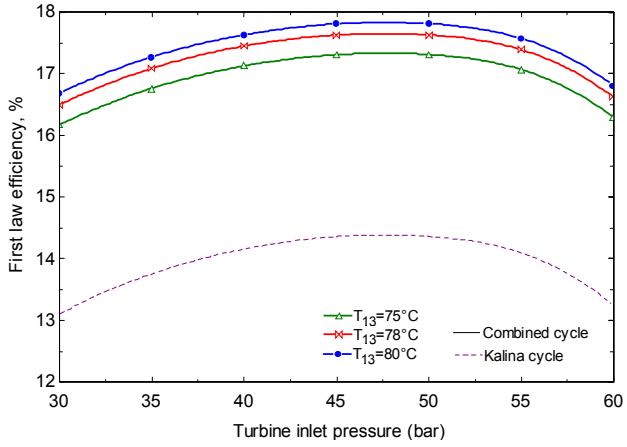

Figure 4: Effect of turbine inlet pressure on the Kalina and combined cycle energy efficiencies for several evaporator exit temperatures

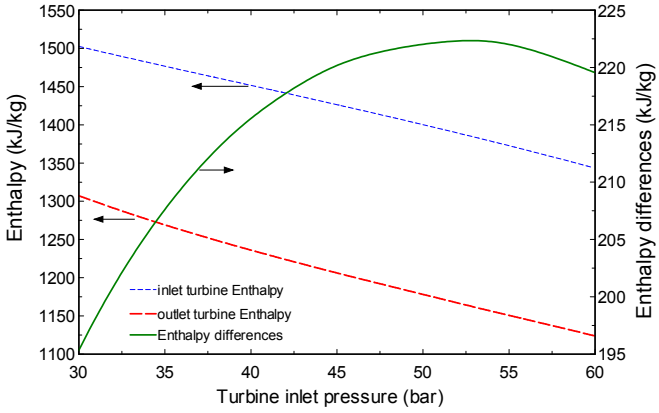

Figure 5: Effect of turbine inlet pressure on the turbine inlet and outlet specific enthalpy values and their differences

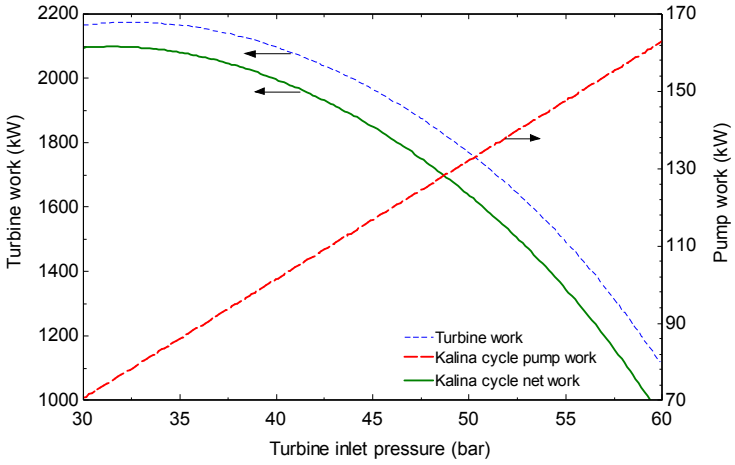

Figure 6: The effect of turbine inlet pressure on the cycle work

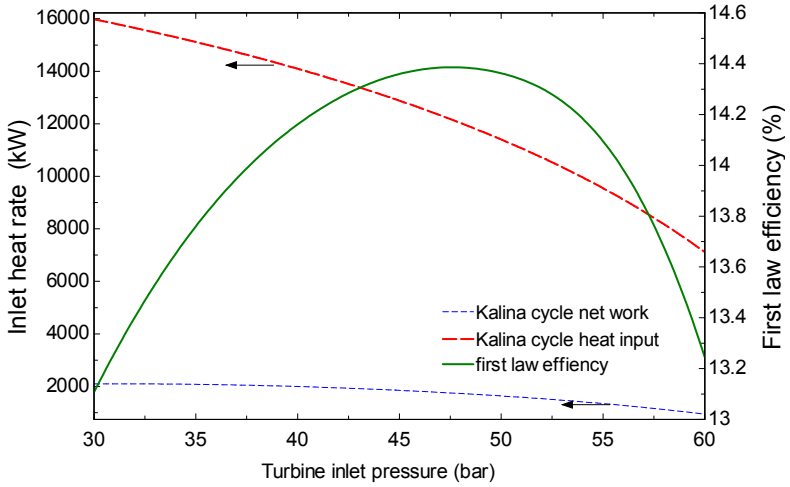

Figure 7: Effect of turbine inlet pressure on performances of the cycles

Figure 8 shows variations in the mass flow rates of the solution passing through the turbine and the hot water versus the turbine inlet pressure. Both the hot water and ammonia-water solution mass flow rates are seen in Figure 8 to decrease as the turbine inlet pressure increases. The first effect is due to a reduction in the cycle heat input rate and the second to the difference in ammonia concentration at the separator.

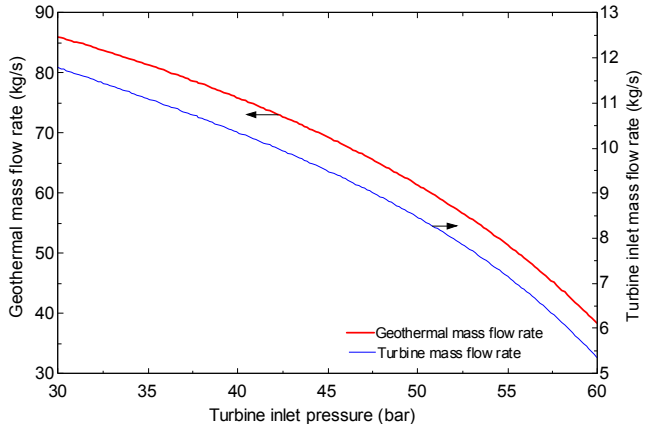

Figure 8: Effect of turbine inlet pressure on the geothermal and turbine inlet mass flow rates

The effect of turbine inlet pressure on the second law efficiencies of the Kalina and combined cycles is shown in Figure 9 for several values of the temperature of the hot water exiting Evaporator 1. It is observed that, at each temperature, there exists a pressure at which the second law efficiency is maximized. It is observed in Figure 9 that the trend of second law efficiency differs from that of the first law efficiency, in particular for the case of the Kalina cycle. It is also evident from Figure 6 that the second law efficiency is lower at higher temperatures of the hot water exiting Evaporator 1. Among the combined cycle components, the highest exergy destruction (10.82% of the total) occurs in Evaporator 1.

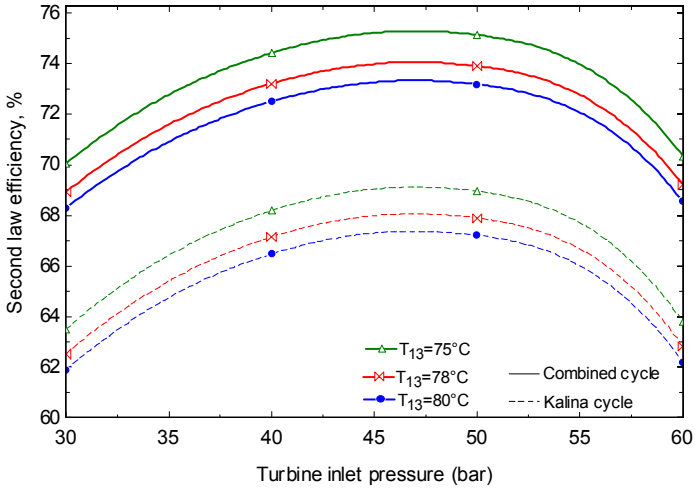

Figure 9: Effect of turbine inlet pressure on the exergy efficiencies of the Kalina and combined cycles for several evaporator exit temperatures

Figure 10 shows the effect of the temperature of the hot water exiting Evaporator 1 on the first and second law efficiencies for a given value of turbine inlet pressure. It is observed that, as the hot water temperature increases, the first law efficiency increases and the second law efficiency decreases. The results can be explained considering the variations of the combined cycle input heat rate, input and output exergy rates and net work rate, as illustrated in Figs. 11 and 12.

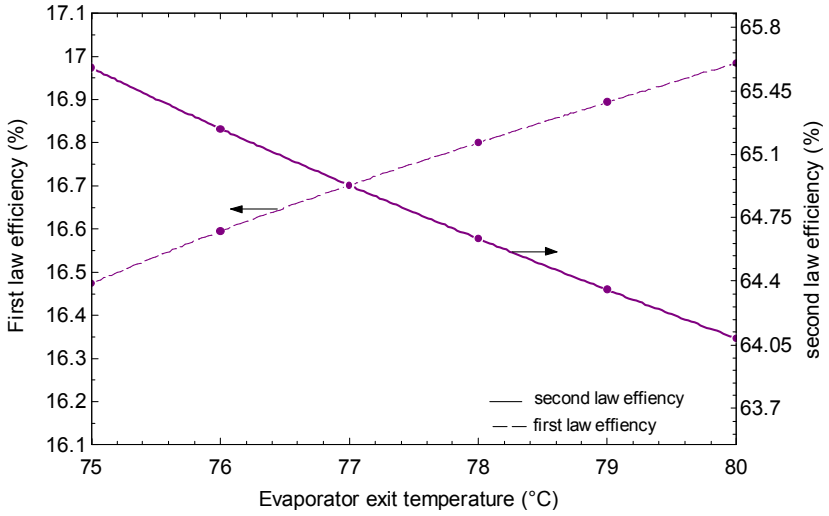

Figure 10: Effect of evaporator exit temperature on first and second law efficiency

The effect of turbine inlet pressure on the production rate of pure water is shown in Fig. 13 for several values of the hot water temperature exiting the evaporator. It is observed that a higher turbine inlet pressure leads to a lower mass flow rate of pure water, and this is because of the lower values of geothermal water flow rate (Figure 8). In fact the reduced geothermal water mass flow rate causes a lower lithium bromide-water mass flow rate in the absorption heat transformer cycle.

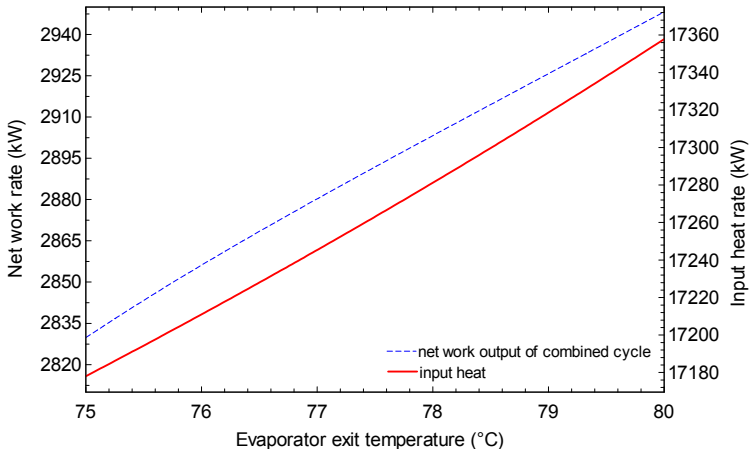

Figure 11: Effect of evaporator exit temperature on net work rate and input heat rate for the combined cycle

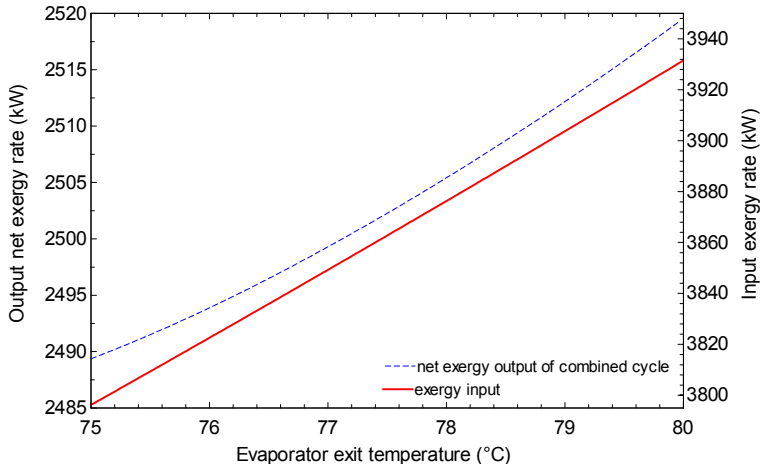

Figure 12: Effect of evaporator exit temperature on net work rate and input heat rate for the combined cycle

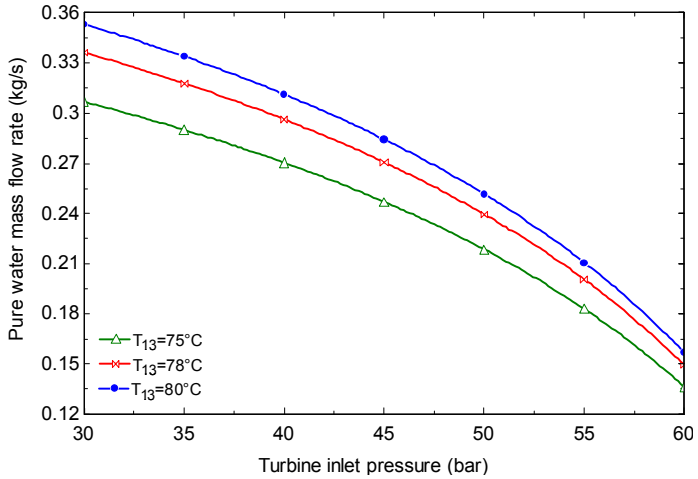

Figure 13: Effect of turbine inlet pressure on the production rate of pure water

Figure 14 shows the effect of turbine inlet pressure on the first law efficiency for several values of ammonia concentration. It is observed that at any ammonia concentration, an optimum pressure exists at which the first law efficiency is maximized. A comparison of Figs. 14 and 8 suggests it is advantageous to have a higher concentration for the solution exiting Evaporator 1, because with higher concentration the efficiency is high and the required geothermal flow rate is low.

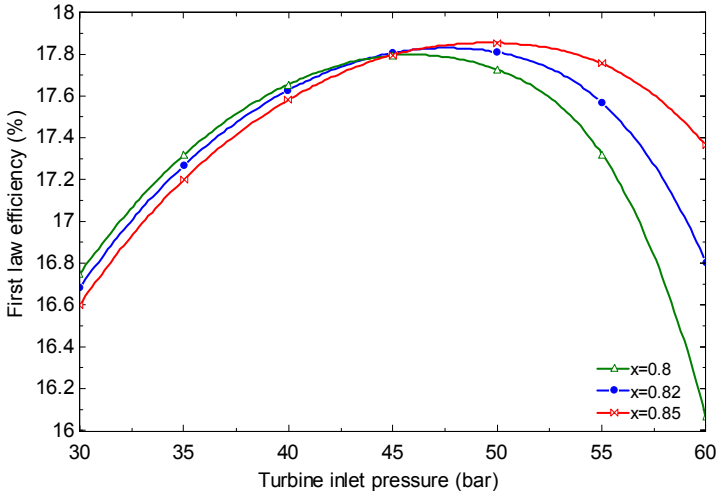

Figure 14: Effect of turbine inlet pressure on the first law efficiency for several values of ammonia concentration

The effect of temperature of hot water exiting Evaporator 1 on the pure water production rate as well as the required geothermal water flow rate is depicted in Figure 15, which indicates that the pure water production rate is increased with increasing temperature due to the increase in lithium bromide-water solution mass flow rate.

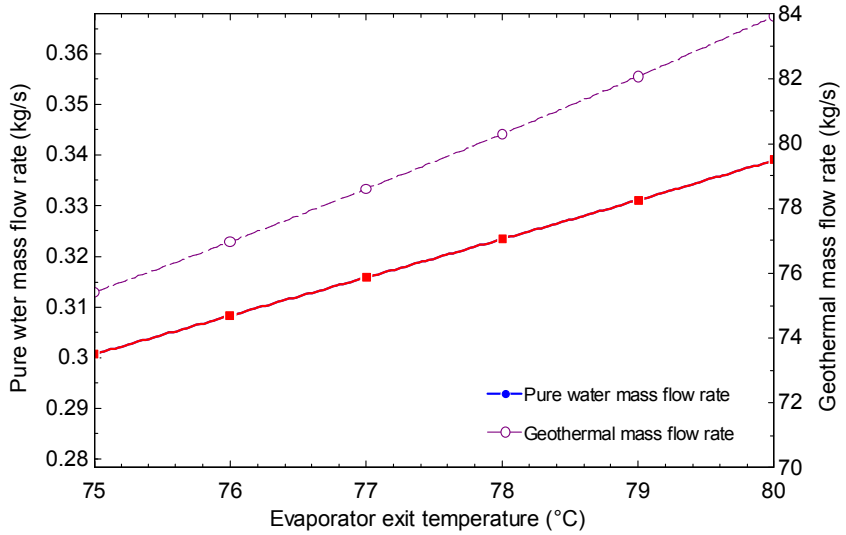

Figure 15: Effect of temperature of hot water exiting Evaporator 1 on the pure water production rate

6. Conclusions

The proposed cycle is an interesting way of utilizing geothermal energy in producing electrical power and pure water simultaneous effective thermodynamically than conventional geothermal power plants. In addition, the proposed system produces pure water. Specifically, the proposed cycle produces 2.94 MW of electrical power and 0.34 kg/s pure water using geothermal water with a mass flow rate of 89 kg/s at a temperature of 124^{o}C. Additional conclusions that can be drawn from the results follow:

- The proposed cycle, which is a combination of Kalina cycle with an ammonia–water working fluid and a heat transformer cycle with lithium bromide–water working fluid, can beneficially substitute for conventional geothermal power plants. The production of pure water by the proposed cycle is another advantage for the proposed cycle. The first and second law efficiencies of the proposed cycle are around 24% and 13% higher than the corresponding values for the Kalina cycle.
- The first and second law efficiencies are maximized at particular values of turbine inlet pressure. The maximum values increase with increasing ammonia concentration at the Evaporator 1 outlet and increasing turbine inlet pressure.
- As the hot water temperature increases at the outlet of Evaporator 1, the first law efficiency increases and the second law efficiency decreases. However, a higher temperature is suggested for the hot water exiting Evaporator1, based on the second law efficiency, which is a more meaningful criteria.
- As the turbine inlet pressure increases and/or the hot water temperature at the exit of Evaporator 1 decreases, the produced mass flow rate of pure water decreases.
- Evaporator 1 makes the highest contribution to the cycle exergy destruction, suggesting that more attention is needed in the design of this component.

It should be noted that in the present work only the thermodynamic aspect of the proposed cycle is investigated. However, considering the economics aspect of the processes is very helpful before taking any action.

References

1. Shi, X. and Che, D., "A combined power cycle utilizing low-temperature waste heat and LNG cold energy"', Energy Conversion and Management, 2009, Volume 50, pp. 567-575.
2. Vidal, A., Best, R., Rivero, J. and Cervantes, J., "Analysis of a combined power and refrigeration cycle by the exergy method", Energy, 2006, Volume 31, pp. 3401-3414.
3. Padilla, R.V., Demirkaya, G., Goswami, D.Y., Stefanakos, E. and Rahman, M.M., "Analysis of power and cooling cogeneration using ammonia-water mixture", Energy, 2010, Volume 35, pp. 4649-4657.
4. Wang, J., Dai, Y., Zhang, T. and Ma, S., "Parametric analysis for a new combined power and ejector-absorption refrigeration cycle", Energy, 2009, Volume 34, pp. 1587-1593.

5. Wang, J., Dai, Y. and Gao, L., "Parametric analysis and optimization for a combined power and refrigeration cycle", Applied Energy, Combustion and Flame, 2008, Volume 113, pp. 135-146.
6. Tamm, G., Goswami, D.Y., Lu, S. and Hasan, A.A., "Theoretical and experimental investigation of an ammonia-water power and refrigeration thermodynamic cycle", Solar Energy, 2004, Volume 76, pp. 217-228.
7. Lolos, P.A. and Rogdakis, E.D., "A Kalina power cycle driven by renewable energy sources", Energy, 2009, Volume 34, pp. 457-464.
8. Maloney, J.D. and Robertson, R.C., "Thermodynamic study of ammonia-water heat power cycles", 1953, Report CF-53-8-43, Oak Ridge National Laboratory, U.S.
9. Ibrahim, O.M. and Kleins, S.A., "Absorption power cycle", Energy, 1996, Volume 21, pp. 21-27.
10. Kalina, Al., "Combined cycle waste heat recovery power systems based on a novel thermodynamic energy cycle utilizing low-temperature heat for power generation", Proceeding of the ASME/joint power generation conference, 1983, pp. 83-JPGC-GT-3.
11. Kalina, Al. "Combined cycle system with novel bottoming cycle", ASME J ENG Gas Power, 1984, Volume 106, pp. 737-742.
12. Kalina, A. and Leibowitz, H.M., "Application of the Kalina technology to geothermal power generation", Geothermal Resources Council Transactions, 1989, Volume 13, pp. 605-611.
13. El-Sayed, Y.M. and Tribus, M.A., "A theoretical comparison of the Rankine and Kalina cycle", ASME Special Publications, AES-1, 1985, pp. 97-102.
14. Stecco S.S. and Desideri, U., "Thermodynamic Analysis of the Kalina Cycles: Comparisons, Problems, Perspectives", *ASME Paper 89-GT-149*, presented at the 34th ASME International Gas Turbine and Aeroengine Congress and Exposition, June 4-8, Toronto, Canada,1989 .
15. Martson, C.H., ASME paper, 89-GT-218, Fairfield, NJ, 1989.
16. Desideri, U. and Bidini, G., "Study of possible optimization criteria for geothermal power plants", Energy Convers. Mgmt, 1997, Volume 38, pp. 1681-1691.
17. Dejfors, C., Thorin, E. and Svedberg, G., "Ammonia-water power cycles for direct-fired cogeneration applications", Energy Convers. Mgmt, 1998, Volume 39, pp. 1675-1681.
18. Jones, D.A., "A Study of the Kalina Cycle System 11 for the Recovery of Industrial Waste Heat with Heat Pump Augmentation", PhD thesis, Auburn University, Auburn, Alabama,2011.
19. Madhawa, H.D., Golubovic, M., Worek, W. and Ikegami, Y., "The performance of the Kalina cycle system (KSC-11) with low-temperature heat sources", J. Energy Resources Technology (ASME), 2007, Volume 129, pp. 243-247.
20. Lolos, P.A. and Rogdakis, E.D., "A Kalina power cycle driven by renewable energy sources", Energy, 2009, Volume 34, pp. 457-464.
21. Bombarda, P., Invernizzi, C.M. and Pietra, C., "Heat recovery from Diesel engine: A thermodynamic comparison between Kalina and ORC cycles", Applied Thermal Engineering, 2010, Volume 30, pp. 212-219.
22. Arslan, O, "Exergoeconomic evaluation of electricity generation by the medium temperature geothermal resources, using a Kalina cycle: Simav case study", International Journal of Thermal Sciences, 2010, Volume 49, pp. 1866-1873.
23. Ogriseck, S., "Integeration of Kalina cycle in a combined heat and power plant, a case study", Applied Thermal Engineering, 2009, Volume 29, pp. 2843-2848.

24. Sekar S., Saravanan R. (2011) “Experimental studies on absorption heat transformer coupled distillation system”, Desalination, Volume 274, pp. 292–301.
25. Rivera W., Siqueiros J. Martínez H. Huicochea A. “Exergy analysis of a heat transformer for water purification increasing heat source temperature”, Applied Thermal Engineering, 2010,Volume 30, pp. 2088-2095.
26. Rivera W., Huicochea A., Martínez H., Siqueiros J., Juárez D. Cadenas E. “Exergy analysis of an experimental heat transformer for water purification”, Energy, 2011,Volume 36, pp. 320-327.
27. Gomri R. “Energy and exergy analyses of seawater desalination system integrated in a solar heat transformer”, Desalination, 2009, Volume 249, pp. 188–196.
28. Gomri R. “Thermal seawater desalination: Possibilities of using single effect and double effect absorption heat transformer systems”, Desalination, 2010,Volume 253, pp. 112–118.
29. Rivera W, Cerezo J, Rivero R, Cervantes J, Best R. “Single stage and double absorption heat transformers used to recover energy in a distillation column of butane and pentane”, Int J Energy Res, 2003, Volume 27, pp. 1279-92.
30. Klein, S.A. and Alvarda, F.R., “Engineering equation solver (EES)”, F-chart software, Madison, WI, 2007.
31. Yari, M., “Exergetic analysis of various types of geothermal power plants”, Renewable Energy, 2010, Volume 35, pp. 112-121.
32. Nag, P.K. and Gupta, V.S.K.S., “Exergy analysis of the Kalina cycle”, Applied Thermal Engineering, 1998, Volume 18, pp. 427-439.
33. DiPippo, R., “Second Law assessment of binary plants generating power from low-temperature geothermal fluids”, Geothermics, 2004, Volume 23, pp. 565-586.
34. A.Bejan, G.Tsatsaronis, M.Moran, , “Thermal design and optimization” New York: John Wiley and Sons Inc, 1996.
35. Misra RD, Sahoo PK, Gupta A. Thermoeconomic evaluation and optimization of an aqua-ammonia vapour-absorption refrigeration system. International Journal of Refrigeration, 2006, Volume 29,pp.47-59.
36. Rossa JA, Bazzo E. Thermodynamic modeling of an ammonia-water absorption system associated with a microturbine. International Journal of Thermodynamics 2009, Volume12,pp.38-43.